

22. H. B. Osborne, C. Sardet, A. Helenius, *Eur. J. Biochem.* **44**, 383 (1974).
23. M. Seigneuret, J.-M. Neumann, J.-L. Rigaud, *J. Biol. Chem.* **266**, 10066 (1991).
24. J. L. Oudar and H. L. Person, *Opt. Commun.* **15**, 258 (1976).
25. J. L. Oudar, *J. Chem. Phys.* **67**, 446 (1977).
26. Y. Kawabe, H. Ikeda, T. Sakai, K. Kawasaki, *J. Mater. Chem.* **2**, 1025 (1992).
27. J. P. Hermann and J. Ducuing, *J. Appl. Phys.* **45**, 5100 (1974).
28. M. Ponder and R. Mathies, *J. Phys. Chem.* **87**, 5090 (1983).
29. F. Meyers, J.-L. Brédas, J. Zyss, *J. Am. Chem. Soc.* **114**, 2914 (1992).
30. L. Onsager, *ibid.* **58**, 1486 (1936).
31. M. W. Wong, K. B. Wiberg, M. J. Frisch, *ibid.* **115**, 1078 (1993).
32. C. E. Dykstra and P. G. Jasien, *Chem. Phys. Lett.* **109**, 388 (1984).
33. G. J. B. Hurst, M. Dupuis, E. Clementi, *J. Chem. Phys.* **89**, 385 (1988).
34. S. R. Marder, C. B. Gorman, L.-T. Cheng, B. G. Tiemann, *Proc. Soc. Photo-Opt. Instrum. Eng.* **1775**, 19 (1993).
35. C. B. Gorman and S. R. Marder, *Proc. Natl. Acad. Sci. U.S.A.*, in press.
36. S. R. Marder *et al.*, *J. Am. Chem. Soc.* **115**, 2524 (1993).
37. F. Simm, S. Chin, M. Dupuis, J. E. Rice, *J. Phys. Chem.* **97**, 1158 (1993).
38. We dedicate this report to Leo De Maeyer on the occasion of his retirement. Supported by the Belgian National Fund for Scientific Research (FNRS/NFWO) (E.H. and K.C.), the Belgian Prime Minister Office of Science Policy under the Interuniversity Attraction Pole on Supramolecular Chemistry and Catalysis, and the Impulse Program on Information Technology (IT/SC/22).

28 June 1993; accepted 7 September 1993

Single Molecules Observed by Near-Field Scanning Optical Microscopy

Eric Betzig and Robert J. Chichester

Individual carbocyanine dye molecules in a sub-monolayer spread have been imaged with near-field scanning optical microscopy. Molecules can be repeatedly detected and spatially localized (to $\sim\lambda/50$ where λ is the wavelength of light) with a sensitivity of at least 0.005 molecules/(Hz)^{1/2} and the orientation of each molecular dipole can be determined. This information is exploited to map the electric field distribution in the near-field aperture with molecular spatial resolution.

Emerging techniques aimed at single molecule detection (SMD) have potential applications across the physical sciences. SMD represents the ultimate goal in trace chemical analysis (1) and has been proposed as a tool for rapid base-sequencing of DNA (2, 3). SMD of site-specific fluorescent probes attached to, for example, individual membrane bound proteins would permit the investigation of such systems with minimal perturbations introduced by the labeling process and without the averaging of physical properties (such as dipole orientations or spectra) associated with the sampling of larger populations. Furthermore, the sensitivity of such properties to environmental conditions could be exploited to locally probe the immediate surroundings of each individual molecule (4, 5). Finally, SMD would facilitate fundamental studies of the process of fluorescence emission, including the probability of photobleaching and variations in both the excited state lifetime (6) and the angular distribution of emitted radiation which can occur in the vicinity of a dielectric interface (7-9).

Although SMD of molecules with numerous (~ 30) chromophores has been possible for some time (10-12), it is only recently that two different approaches have

been developed for the detection of single chromophore dyes which are of greatest interest for the above applications. The first involves spectral isolation at low temperature (~ 1.5 K) of a single absorption (4) or fluorescence excitation (5) peak in the wings of an inhomogeneously broadened line. Of more general applicability are efforts involving SMD in solution, where the central problem of isolating the molecular fluorescence signal from background luminescence and Raman scattering is overcome by reducing the excitation volume to the smallest possible size, either with levitated microdroplets (1) or within a thin flow cell (3). Remaining problems with these latter methods include a low measurement bandwidth, photobleaching of the molecule in the course of detection, and a limited degree of confidence in each potential detection event.

To achieve further gains in SMD, we have reduced the optical excitation volume even further—indeed, to subwavelength proportions in all three dimensions. This is accomplished using illumination mode near-field scanning optical microscopy (NSOM) (13). In this technique, visible light is funneled through a small aperture (100 nm in these experiments) at the end of a sharp and otherwise opaque probe (14) to transversely illuminate at most an aperture sized region of the sample at any one time.

Confinement of the detection volume in the axial direction is achieved with a photon-counting avalanche photodiode (APD) of small active area (100 μm), high quantum efficiency (55% at 630 nm), and low dark noise (seven counts per second) which is confocal with the aperture in the image plane of the far-field objective used to collect the fluorescence emission from individual molecules (15). Further axial confinement of this signal may be afforded by enhanced fluorescence excitation from evanescent fields of large amplitude predicted to exist in the near field of a subwavelength aperture (16). Complete images of the lateral distribution of molecules with transverse resolution on the order of the aperture size can then be generated by raster scanning the sample relative to the probe and recording the fluorescence signal obtained at each point (17).

As an initial test of this approach to SMD, a sample was prepared by spreading a dilute methanol solution of the lipophilic carbocyanine dye diIC₁₂(3) (Molecular Probes #D-383) across a cover slip previously spin coated with an ~ 30 -nm-thick polymethylmethacrylate (PMMA) film to achieve a calculated areal density of ~ 23 molecules μm^{-2} (18). DiIC₁₂(3) was chosen for its photostability, large absorption cross section, and significance as a membrane probe (19). PMMA was used because it was empirically observed to enhance both the apparent quantum yield and adhesion of the individual molecules. The sample was then imaged with the NSOM system described in (13) and (15), with the results shown in Fig. 1 as six images (20) of the same region obtained sequentially but under differing polarization conditions.

A wealth of information can be extracted from this data. We begin with the evidence that the individual structures observed represent luminescence from single molecules. The arguments are fivefold. First, the areal density of ~ 3.5 molecules μm^{-2} measured from Fig. 1A is only about a factor of 6 lower than that calculated above, with the discrepancy probably attributable to considerable unevenness in the spreading process, photobleaching in the original solution or on the substrate, and nonradiative energy transfer from certain molecules in unfavorable local environments. Second, the density changes linearly over almost three orders of magnitude with changes in the concentration of the solution. Third, the peak signal observed (for example, 380 counts in 10 ms for molecule b in Fig. 1D) is consistent with the emission expected from a single diIC₁₂(3) molecule under the known excitation conditions (21). Fourth, each structure in Fig. 1 has a well-defined dipole orientation as discussed below. Finally,

AT&T Bell Laboratories, 600 Mountain Avenue, Murray Hill, NJ 07974.

bleaching does not occur as a gradual dimming of each structure, but as a discrete and total extinction of luminescence (for example, molecule a between Fig. 1, A and B).

Confident then that we have achieved SMD combined with superresolution imaging, we can estimate our detection limits. We first note that the reduced probe volume of the NSOM geometry results in a background level (~ 20 counts in 10 ms) small compared to the optimum signal from an individual molecule, so that the shot noise corresponding to ~ 0.005 molecules/(Hz)^{1/2} dominates (22). Furthermore, each individual pixel above background represents a detection event, and $\sim 50\%$ of the molecules remained photoactive after 10 images (23), indicating an ability to detect the same molecule ~ 300 times with a mean signal to noise ratio ~ 15 within one half-life due to photobleaching ($\tau_{1/2}$). Alternatively, these numbers suggest that $\sim 10^5$ counts per molecule can be extracted within $\tau_{1/2}$, making near-field optical spectroscopy of a single molecule a definite possibility. It is also important to note that these results were obtained under ambient conditions with a reasonably simple and inexpensive system. In an oxygen reduced environment designed to reduce photobleaching, larger integrated yields may be anticipated.

Perhaps even more surprising initially than this sensitivity was the observation that the molecules do not appear as identical peaks of width comparable to the aperture size, but rather as a distribution of symmetric peaks (molecule b in Fig. 1D), ellipsoidal peaks (molecule c in Fig. 1E), rings (molecule d in Fig. 1C), arcs (molecule e in Fig. 1B), and double arcs (molecule f in Fig. 1F). In retrospect, and with the aid of the sketch in Fig. 2, such results are understandable when we recall that a dye molecule acts as an electric dipole in its interaction with an incident electromagnetic field, so that each molecule in the field of view serves as a point detector excited by the square of that component of the electric field \mathbf{E} emerging from the aperture that is along the molecular dipole direction \mathbf{p} . The total observed intensity is then given by:

$$I(x, y, \theta, \phi) = \Lambda(\theta, \phi, \psi = \psi_0, d = d_0) \times |\mathbf{p}(\mathbf{x} = \mathbf{x}_0, \theta, \phi) \cdot \mathbf{E}(x, y, z = z_0)|^2 \quad (1)$$

where $\cos\theta = \hat{\mathbf{p}} \cdot \hat{\mathbf{e}}_z$, $\cos\phi \sin\theta = \hat{\mathbf{p}} \cdot \hat{\mathbf{e}}_x$, and Λ is a collection efficiency correction factor for an objective of numerical aperture $NA = n \sin\psi$ which depends upon the vertical orientation θ and the distance d of the dipole from the substrate-air interface (9).

With high NA collection ($\psi \rightarrow \pi/2$)

and no analyzer before the detector (Fig. 1, A and D through F), Λ is roughly independent of θ , ϕ , and d at a purely dielectric interface (9), so that the excitation term $|\mathbf{p} \cdot \mathbf{E}|^2$ is the dominant variable. Consequently, molecules in Fig. 1 with dipole orientations approximately aligned along the axes defined by the excitation polarization [which is fixed (14, 24) in Fig. 1, E and F] and the normal to the plane of the aperture provide maps of the square of the components of the electric field along each of these directions. In particular, molecule c in Fig. 1E maps E_x^2 and molecule f in Fig. 1F maps E_z^2 . These maps are shown in expanded form in the center of Fig. 3 and compared to the squared fields predicted by Bethe (25) [with corrections by Bouwkamp (26)] to emerge from a small aperture ($a/\lambda \ll 1$) in an infinitesimally thin, perfectly conducting planar screen.

From this comparison, we conclude that the predictions of the model are quite good, despite its obvious limitations. Furthermore, by using the model to plot E_x^2 and E_z^2 for several z/a values as shown in Fig. 3, and given the known aperture radius $a \sim 50$ nm, we determine the dipole-aperture separation of $z \sim 15$ nm for molecules c and f. This is consistent with the feedback distance estimated from shear force approach curves (27), assuming the chromophore in each case is resting near the upper surface of the PMMA. Thus, we can transversely

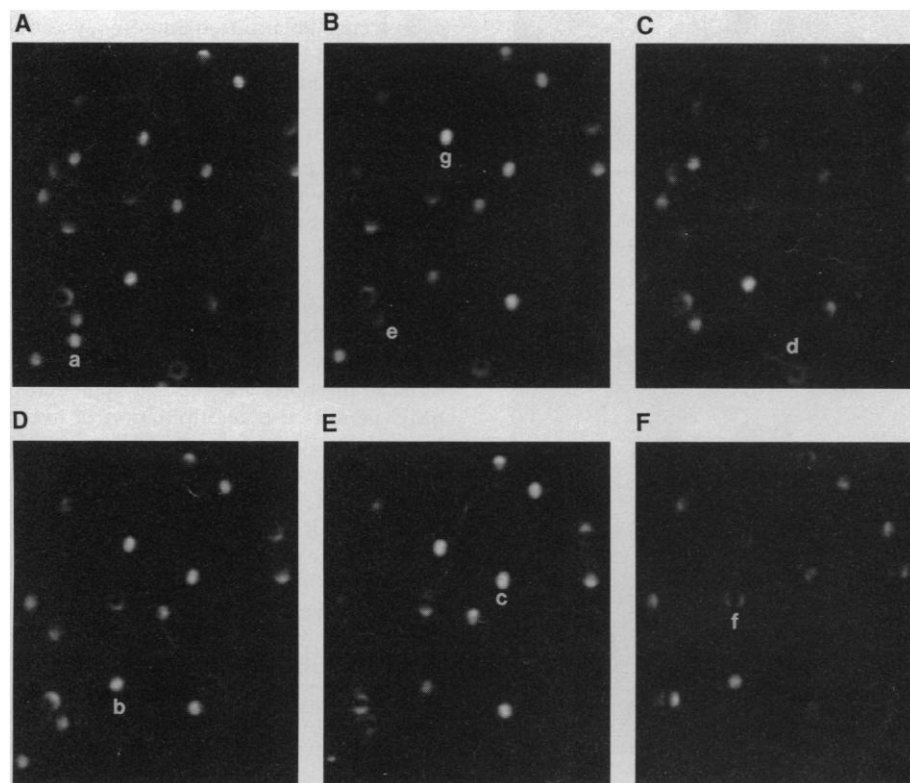


Fig. 1. Six sequential images of the exact same field of individual carbocyanine dye molecules as detected by near-field optical fluorescence microscopy. The excitation polarization is random in (A) through (D) and linear along y and x , respectively, in (E) and (F). The emission polarization is measured along y and x in (B) and (C), respectively, and not measured otherwise. Certain molecules have been labeled for discussion in the text.

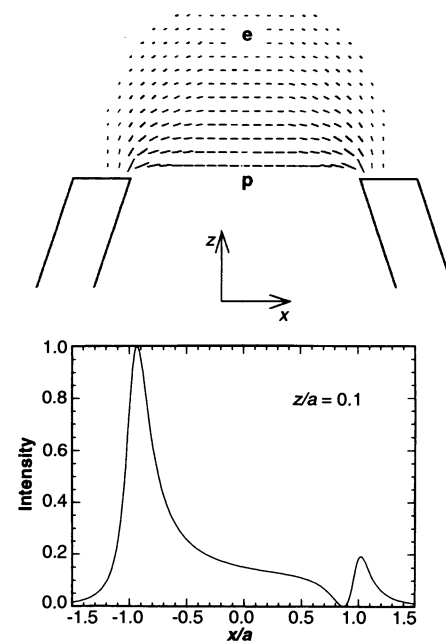


Fig. 2. (Top) Schematic view of a molecular dipole \mathbf{p} (arrow) at a particular orientation within the electric field pattern \mathbf{E} of a subwavelength aperture. (Bottom) Resulting intensity I versus x for this particular orientation, proportional to the square of the component of \mathbf{E} along \mathbf{p} ($I \propto |\mathbf{p} \cdot \mathbf{E}|^2$).

resolve molecules to $\sim\lambda/10$ (that is, to within $\sim a$), transversely localize molecules to at least $\lambda/40$ (that is, the pixel size), and axially localize molecules to at least $\lambda/100$.

The experimental field maps in the center of Fig. 3 are also of interest because they represent a direct determination of the electric field distribution in a subwavelength aperture at optical frequencies. As such, they may aid in developing an understanding of unusual optical contrast effects observed in the near field (28).

For those images where the excitation polarization is not fixed but varies randomly in time (Fig. 1, A through D), the intensity is given by a time average of the suitably modified version of Eq. 1, yielding the average of the two intensities obtained under the orthogonal fixed polarizations.

Thus, for example, the average of the double arcs for molecule *f* in each of Fig. 1, E and F, yields the asymmetric rings in Fig. 1, A and D. Once excited, the emission pattern of each molecule depends only on its orientation. Consequently, for molecules such as *f* predominantly aligned along \hat{e}_z , the polarization of radiation emitted to the far field remains circularly symmetric, so that the ring appearance is preserved even when a linear polarizer is inserted before the APD to analyze the state of this emission (Fig. 1, B and C). However, for molecules such as *b* and *g* aligned along \hat{e}_x and \hat{e}_y , respectively, the far-field emission is predominantly polarized along *p*, resulting in the alternately bright and dim peaks in Fig. 1, B and C, reminiscent of those observed under polar-

ized excitation in Fig. 1, E and F.

Given the good agreement of the model to the data for molecular dipoles aligned along the principle axes, we can extend it to predict the patterns expected to be observed under other dipole orientations. By doing this, we find that patterns corresponding to every pair of structures in Fig. 1, E and F, can be generated, thereby allowing us to determine the orientation of every molecular dipole in the field of view. Working in this fashion, the schematicized dipole orientation map in Fig. 4 was constructed.

From this map, we first discover that there is little if any preferential orientation to the chromophores of the molecules as they rest upon the PMMA. Second, the good fit of the data to the model for each molecule (in terms of intensity as well as shape) suggests that the apparent absorption cross section and quantum yield are quite uniform (taking into account the orientational dependence), which provides further evidence of SMD. Finally, we note that it is possible to use these same methods in conjunction with the data in Fig. 1, B and C, to determine the emission dipole orientations as well as the absorption dipole directions shown here.

Average orientations of large ensembles of molecules have been measured previously by conventional (19) and evanescent (8) fluorescence polarization microscopy as well as by second-harmonic generation (29). In contrast, in Fig. 4 the fixed dipole orientations of individual molecules have been determined. In addition, however, this information is provided along with an unsurpassed ability to resolve closely packed molecules and localize individual molecules. On top of this, the results of the model can be extended to all *z* values as in Fig. 3 as well as all orientations to determine the depth of each molecule for those molecules within a few tens of nanometers from the surface. In short, the NSOM approach to SMD permits the determination of five of the six degrees of freedom for each molecule, with only the optically inactive rotation around the dipole axis not at our disposal. This may have important implications for the study of receptors in membranes and the development of organic non-linear devices.

REFERENCES AND NOTES

1. W. B. Whitten, J. M. Ramsey, S. Arnold, B. V. Bronk, *Anal. Chem.* **63**, 1027 (1991).
2. J. H. Jett *et al.*, *J. Biomol. Struct. Dynam.* **7**, 301 (1989).
3. E. B. Shera, N. K. Seitzinger, L. M. Davis, R. A. Keller, S. A. Soper, *Chem. Phys. Lett.* **174**, 553 (1990).
4. W. E. Moerner and L. Kador, *Phys. Rev. Lett.* **62**, 2535 (1989); L. Kador, D. E. Horne, W. E. Moerner, *J. Phys. Chem.* **94**, 1237 (1990).
5. M. Orrit and J. Bernard, *Phys. Rev. Lett.* **65**, 2716

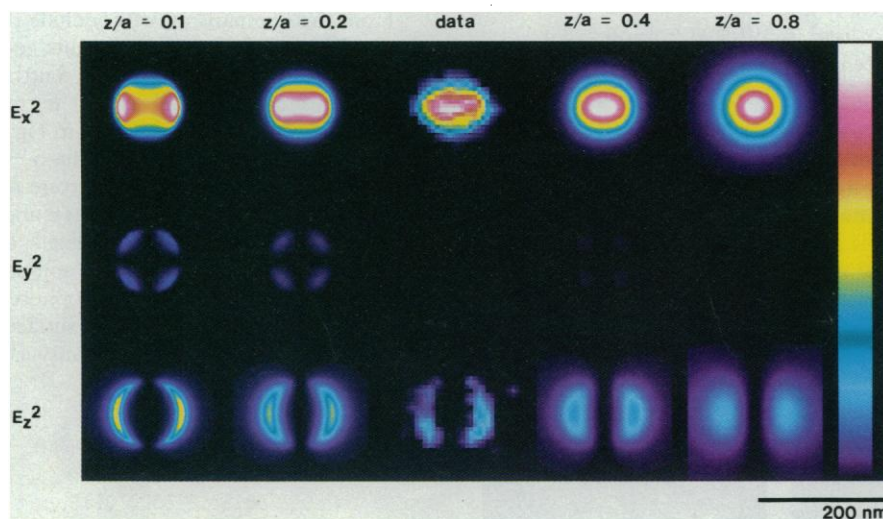


Fig. 3. Squared components of the electric field predicted (24, 25) to exist at various normalized distances (*z/a*) from a subwavelength diameter aperture, as compared to profiles (center) observed in Fig. 1 for molecules *c* (E_x^2) and *f* (E_z^2).

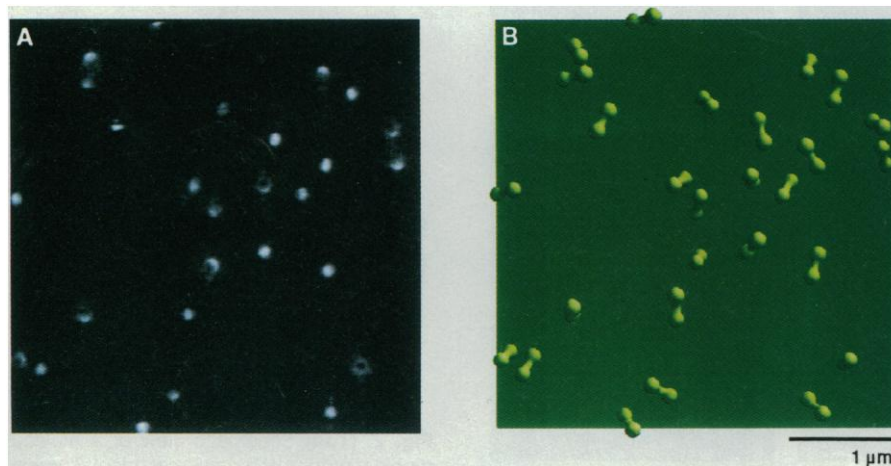


Fig. 4. (A) Extended $4 \times 4 \mu\text{m}$ image of the scan area under random polarization. (B) Stylized map indicating the dipole orientations of molecules in (A) as inferred from polarization data and the model in Fig. 3. Each dipole is represented as a dumbbell centered at the molecular position, with a length determined by the projection of the dipole onto the *xy* plane, and an angular orientation determined by ϕ .

- (1990); H. Talon, L. Fleury, J. Bernard, M. Orrit, *J. Opt. Soc. Am. B* **9**, 825 (1992).
6. K. H. Drexhage, *J. Lumin.* **12**, 693 (1970).
 7. W. Lukosz and R. E. Kunz, *J. Opt. Soc. Am.* **67**, 1607 (1977); *ibid.*, p. 1615; W. Lukosz, *ibid.* **69**, 1495 (1979).
 8. T. P. Burghardt and N. L. Thompson, *Biophys. J.* **46**, 729 (1984); N. L. Thompson, H. M. McConnell, T. P. Burghardt, *ibid.*, p. 739.
 9. E. H. Hellen and D. Axelrod, *J. Opt. Soc. Am. B* **4**, 337 (1987).
 10. T. Hirshfeld, *Appl. Opt.* **15**, 2965 (1976).
 11. D. C. Nguyen, R. A. Keller, J. H. Jett, J. C. Martin, *Anal. Chem.* **59**, 2158 (1987).
 12. K. Peck, L. Stryer, A. N. Glazer, R. A. Mathies, *Proc. Natl. Acad. Sci. U.S.A.* **86**, 4087 (1989).
 13. E. Betzig and J. K. Trautman, *Science* **257**, 189 (1992).
 14. ———, T. D. Harris, J. S. Weiner, R. L. Kostelak, *ibid.* **251**, 1468 (1991).
 15. The entire optical path for these experiments was as follows: (i) laser light source (green He-Ne, $\lambda = 543.5$ nm for random polarization and emission polarization images, Kr⁺, $\lambda = 530.9$ nm for excitation polarization); (ii) rotatable $\lambda/2$ plate; (iii) rotatable $\lambda/4$ plate (for manipulation of excitation polarization at the aperture); (iv) $\lambda = 535$ nm, $\Delta\lambda = 35$ -nm bandpass filter (Omega Optical #535DF35, for rejection of spontaneous emission noise from laser); (v) coupling objective into fiber (Newport Corp. 10 \times , 0.25 NA); (vi) single mode fiber (~ 1 m, 3M Corp. #FS-VS-2211) with 100-nm aperture at tapered, Al coated distal end; (vii) sample (see text); (viii) immersion oil ($n = 1.518$, Zeiss type 518C); (ix) 100 \times , 1.25 NA objective (Zeiss #44 02 80); (x) Schott glass $\lambda = 570$ -nm-long pass filter (for rejection of excitation light); (xi) dichroic sheet polarizer (Melles Griot #03 FPG 001, for emission polarization images only); (xii) 160-mm-focal length tube lens of Zeiss Axioskop; (xiii) $\lambda = 633$ -nm-holographic notch plus filter (Kaiser Optical #HNPF-633-1.0, for rejection of light associated with shear force feedback detection); (xiv) $\lambda = 600$ nm, $\Delta\lambda = 40$ -nm bandpass filter (Corion #S40-600, for further rejection of excitation and shear force wavelengths); and (xv) photon counting APD (EG&G #SPCM-200-PQ).
 16. U. Dürig, D. W. Pohl, F. Rohner, *J. Appl. Phys.* **59**, 3318 (1986).
 17. The potential of near-field fluorescence microscopy has been recognized for some time, with fluorescence detection through subwavelength apertures first reported in E. Betzig, A. Lewis, A. Harootyan, M. Isaacson, and E. Kratschmer [*Biophys. J.* **49**, 269 (1986)], and U. Ch. Fischer [*J. Opt. Soc. Am. B* **3**, 1239 (1986)]. An application demonstrating the current capabilities of fluorescence NSOM as applied to cell biology (in particular, cytoskeletal imaging) can be found in E. Betzig, R. J. Chichester, F. Lanni, and D. L. Taylor [*Bioimaging*, in press].
 18. Five microliters of a 2.5 nM solution of diI_{C₁₂}(3) was spread over the 18 \times 18 mm area of the cover slip to result in the areal density quoted.
 19. D. Axelrod, *Biophys. J.* **26**, 557 (1979).
 20. Each 2.3 \times 2.7 μ m image in Fig. 1 was extracted from a 256 \times 256 pixel image covering 4 \times 4 μ m taken with a pixel integration time of 10 ms.
 21. The equivalent excitation power extrapolated back to the aperture corresponds to $\sim 3 \times 10^{10}$ counts s⁻¹ at the APD. With an extinction coefficient $\epsilon \sim 1.5 \times 10^5$ M⁻¹ cm⁻¹ for diI_{C₁₂}(3), an assumed quantum yield of 0.2, and an estimated collection efficiency (including filters) of 0.2, we then expect $\sim 5 \times 10^3$ counts s⁻¹ per molecule. Although this is almost an order of magnitude less than the peak signal actually measured, the discrepancy is understandable in view of the uncertainties in the above numbers, the fact that the molecular interaction with the aperture field is more complicated than this calculation would suggest (that is, Figs. 2 and 3), and the likelihood that evanescent fields contribute significantly to the signal (16).
 22. With an optimum count rate of $\sim 4 \times 10^4$ s⁻¹ from a single molecule, the Poisson distributed shot noise is $(4 \times 10^4)^{1/2} = 2 \times 10^2$ in a 1 Hz bandwidth. This

is 1/200 of the molecular signal. Thus, for other bandwidths we more generally specify the resultant shot noise limited sensitivity as ~ 0.005 molecules/(Hz)^{1/2}. This sensitivity was achieved with 0.4 mW of excitation power at $\lambda = 543.5$ nm coupled into the cleaved proximal end of the single mode fiber. Higher sensitivity might be achieved at higher power, with the eventual limit being determined by tip heating effects. Alternatively, the sensitivity could be enhanced by increasing the aperture size beyond 100 nm, but with a concomitant loss of spatial resolution and an eventual limit occurring when the background level (which would also increase due to the increasing effective excitation volume) becomes comparable to the shot noise for the measurement bandwidth chosen.

23. Figure 1F is actually the tenth image of the series, since two images each were taken of Fig. 1, B, C, E, and F.

24. E. Betzig, J. K. Trautman, J. S. Weiner, T. D. Harris, R. Wolfe, *Appl. Opt.* **31**, 4563 (1992).
25. H. A. Bethe, *Phys. Rev.* **66**, 163 (1944).
26. C. J. Bouwkamp, *Philips Res. Rep.* **5**, 321 (1950); *ibid.*, p. 401.
27. E. Betzig, P. L. Finn, J. S. Weiner, *Appl. Phys. Lett.* **60**, 2484 (1992).
28. J. K. Trautman *et al.*, *J. Appl. Phys.* **71**, 4659 (1992); E. Betzig *et al.*, *Appl. Phys. Lett.* **61**, 142 (1992).
29. T. F. Heinz, H. W. K. Tom, Y. R. Shen, *Phys. Rev. A* **28**, 1883 (1983).
30. We thank the following people for their valuable suggestions: R. D. Grober, H. F. Hess, T. D. Harris, J. K. Trautman (AT&T Bell Labs); J. Hwang and M. Edidin (Johns Hopkins University); and F. Lanni (Carnegie Mellon University).

15 September 1993; accepted 19 October 1993

Photon Emission at Molecular Resolution Induced by a Scanning Tunneling Microscope

R. Berndt, R. Gaisch, J. K. Gimzewski, B. Reihl, R. R. Schlittler, W. D. Schneider, M. Tschudy

The tip-surface region of a scanning tunneling microscope (STM) emits light when the energy of the tunneling electrons is sufficient to excite luminescent processes. These processes provide access to dynamic aspects of the local electronic structure that are not directly amenable to conventional STM experiments. From monolayer films of carbon-60 fullerenes on gold(110) surfaces, intense emission is observed when the STM tip is placed above an individual molecule. The diameter of this emission spot associated with carbon-60 is approximately 4 angstroms. These results demonstrate the highest spatial resolution of light emission to date with a scanning probe technique.

A diversity of problems concerning the structure, growth, and aspects of the electronic structure of surfaces and interfaces has been addressed with the use of the STM (1). An exciting prospect is to perform local experimentation with individual adsorbed molecules (2). Inelastic processes excited by tunneling electrons, which are known to carry specific information on molecular systems (3), are difficult to observe by conventional STM. They may, however, be investigated by the detection of photons emitted from the tip-sample region (4, 5). The use of STM as an excitation source that is confined to subnanometer dimensions may open an avenue to combine powerful optical techniques with the high spatial resolution of the STM. Here we report spatially resolved photon emission from individual C₆₀ molecules. For hexagonal arrays of C₆₀, we observe the strongest fluorescence when the tip of an STM is centered above an individual molecule. The mapping of this pho-

ton signal shows this emission spot to have a lateral extent of about 4 Å.

The experiments were conducted with a custom-built, low-temperature, ultra-high vacuum (UHV) STM operating at a pressure of 10⁻¹¹ mbar and employing temperatures of 5 and 50 K (6). Low temperatures improve the stability of imaging at elevated currents and voltages. The samples were prepared in situ by UHV sublimation of C₆₀ onto clean, Au(110) 1 \times 2-reconstructed surfaces, followed by annealing to 650 K before cooling. The structural properties of thin layers of C₆₀ have been thoroughly investigated by STM (7). Electrochemically etched W, and Pt, tips were cleaned in the UHV by heating and Ne ion bombardment. Photons were collected with a low *f*-number lens mounted in the cryostat and counted by a cooled photomultiplier. Measurement of the photon signal was performed quasi-simultaneously with the acquisition of constant-current topographs for each image pixel.

A molecularly resolved STM image from a C₆₀ monolayer recorded at a constant current of 4.4 nA and a tip voltage V_t of -2.8 V is shown in Fig. 1A. Similar results were obtained for reverse bias ($V_t = +2.8$ V). The image shows an approximately

R. Berndt, R. Gaisch, W. D. Schneider, Institut de Physique Expérimentale, Université de Lausanne, CH-1015 Lausanne, Switzerland.
J. K. Gimzewski, B. Reihl, R. R. Schlittler, M. Tschudy, IBM Research Division, Zurich Research Laboratory, CH-8803 Rüschlikon, Switzerland.